

Experimental and theoretical structure characterization of two isoniazid derivatives: 2,4-Difluoro-*N'*-isonicotinoylbenzohydrazide and 2,4-dichloro-*N'*-isonicotinoylbenzohydrazide hydrochloride

Floriano P. Silva Jr ^{a,b,*}, Javier Ellena ^c, Marcelle de Lima Ferreira ^d, Yvonne P. Mascarenhas ^c, Marcus V.N. de Souza ^d, Thatyana R.A. Vasconcelos ^d, James L. Wardell ^b, Solange M.S.V. Wardell ^d

^a Laboratório de Bioquímica de Proteínas e Peptídeos, Instituto Oswaldo Cruz, FIOCRUZ 21045-900, RJ, Brazil

^b Instituto de Química, Universidade Federal do Rio de Janeiro, 21945-970 Rio de Janeiro, RJ, Brazil

^c Instituto de Física de São Carlos, Universidade de São Paulo, 13560-970 São Carlos, SP, Brazil

^d Instituto de Tecnologia em Fármacos, Far-Manguinhos, FIOCRUZ, 21041-250 Rio de Janeiro, RJ, Brazil

Received 5 August 2005; received in revised form 14 November 2005; accepted 16 November 2005

Available online 4 January 2006

Abstract

An X-ray and a theoretical study of the structure of the isoniazid derivatives, 2,4-difluoro-*N'*-isonicotinoylbenzohydrazide, **3**, and 2,4-dichloro-*N'*-isonicotinoylbenzohydrazide hydrochloride, [4H⁺, Cl⁻, 2(H₂O)], are reported. Quantum chemical calculations as well as conformational analysis are presented with the isolated cations [3H⁺] and [4H⁺], where the former was protonated in silico to allow direct comparison of results. Supermolecule calculations were also carried out with the asymmetric unit of [4H⁺, Cl⁻, 2(H₂O)], which is comprised of two independent cations (4H⁺), two chloride ions and four water molecules. Our results indicate that the crystal structures, although clearly representing accessible conformations, are highly distorted in comparison to the predicted lower energy conformers in the gas-phase. These distortions are most probably imposed by polar and electrostatic interactions within the crystal packing. In general, the calculated potential energy surfaces (PES) for both isoniazid derivatives are fairly flat, a feature confirmed by the low energetic difference calculated for several conformers corresponding to local minima in PES. Noteworthy, the fluorinated compound [3H⁺] shows an important additional energy barrier for rotation around the bond connecting the halogenated ring to the proximate carbonyl due to a strong internal hydrogen bond involving the fluorine atom.

© 2005 Elsevier B.V. All rights reserved.

Keywords: Isoniazid derivatives; X-ray structure; Supermolecule calculation; Density functional theory; RHF; Potential energy surfaces; Electronic energy

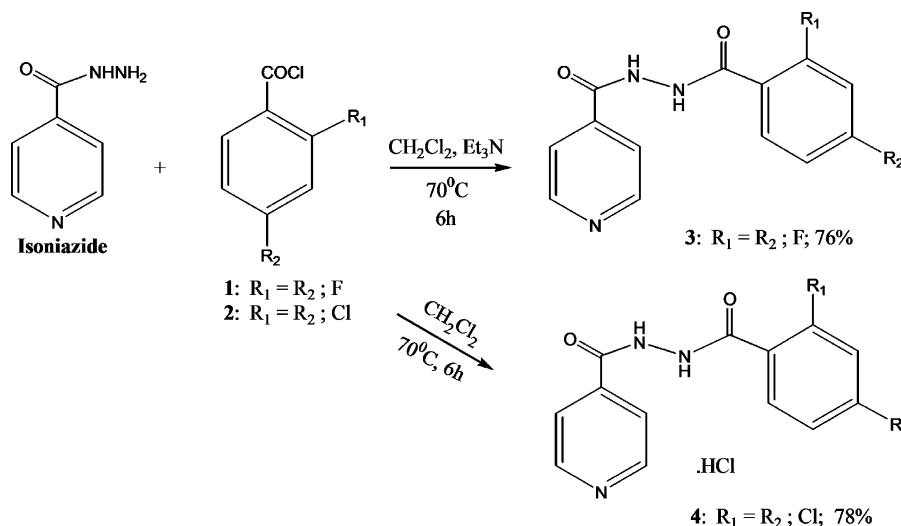
1. Introduction

Tuberculosis (TB) is currently a worldwide problem. This contagious disease kills four people every minute somewhere in the world and amounts to more than two million deaths per year [1]. At present, the accepted treatment of TB involves a combination of the first-line drug, isoniazid, 4-(H₂NNHCO)pyridine, along with pyrazinamide, ethambutol and rifampicin given in combination over 6–9 months [2,3]. Combinations are used to limit the emergence of multiple

drug-resistant (MDR) organisms, which would lead to an ineffective treatment. Several factors have prompted the scientific community to develop new drugs to fight tuberculosis. The most significant of these are (i) the rapid spread of MDR–TB strains resistant to all major anti-tuberculosis drugs in the market and (ii) the association of TB with human immunodeficiency virus (HIV) infection in AIDS. In this paper, we report the X-ray crystallographic and molecular modeling study of two new isoniazid derivatives, obtained from the reactions of isoniazid with 2,4-X₂C₆H₃COCl (**1**: X = F; **2**: X = Cl), see Scheme 1. The compound, 2,4-difluoro-*N'*-isonicotinoylbenzohydrazide, (**3**), and the salt, 2,4-dichloro-*N'*-isonicotinoylbenzohydrazide hydrochloride [4H⁺, Cl], presented minimal inhibitory concentration (MIC) of 10 µg/mL when tested against *Mycobacterium tuberculosis* strain H₃₇Rv (ATCC 27294). A paper with the biological activities of these

* Corresponding author. Address: Fundao Instituto Oswaldo Cruz, Bioquímica e Biologia Molecular, Av. Brasil 4365, Pav. 26, sl. 311, 21045-900 Rio de Janeiro, Brazil. Tel.: +55 21 3865 8157; fax: +55 21 25903 495.

E-mail address: floriano@ioc.fiocruz.br (F.P. Silva).



Scheme 1.

compounds and their analogues has been submitted to a specialist journal [4] and hence these are not reported here.

2. Experimental, theoretical and computational methods

2.1. Synthesis

2.1.1. General

Melting points were determined on a Buchi apparatus and are uncorrected. Infrared spectra were recorded on a Thermo Nicolet Nexus 670 spectrometer in KBr pellets and frequencies are expressed in cm^{-1} . Mass spectra (CG/MS) were recorded on a Agilent Technologies 61530A/5792A mass spectrometer. NMR spectra were recorded on a Bruker Avance 500 spectrometer operating at 500.00 MHz (^1H) and 125.0 MHz (^{13}C), in deuterated dimethyl sulfoxide. Chemical shifts are reported in ppm (δ) relative to tetramethylsilane. Proton and carbon NMR spectra were obtained at room temperature.

2.1.2. Preparations of 2,4-difluoro-*N'*-isonicotinoylbenzohydrazide

The carboxylic acid chloride derivative (1) was prepared by treating 2,4- $\text{F}_2\text{C}_6\text{H}_4\text{CO}_2\text{H}$ (1 g) with thionyl chloride (3 equiv.), *N,N*-dimethylformamide (0.1 equiv.) in dichloromethane (20 mL) at room temperature, under stirring and nitrogen atmosphere. After 6 h, the excess of thionyl chloride was removed and the crude product was used as such in the next stage.

Reaction between (1), isoniazid and triethylamine (equimolar) in tetrahydrofuran (20 mL) at 70°C , under nitrogen atmosphere and stirring for 6h led to the crude product 3 (Scheme 1). Purification by column chromatography on silica gel (0.063–0.2 mm mesh size), eluting with a hexane:ethyl acetate gradient, afforded pure 3.

Yield: 76%; m.p.: 188–189 $^\circ\text{C}$. GC/MS: m/z [M] $^+$: 277; ^1H NMR (500.00 MHz, $\text{DMSO-}d_6$) δ : 10.96 (1H; s; NH); 10.54 (1H; s; NH); 8.80 (2H; d; $J=6.0$ Hz; $\text{H}_{2/}$ and $\text{H}_{6/}$); 7.83 (2H; d; $J=6.0$ Hz; $\text{H}_{3/}$ and $\text{H}_{5/}$); 7.76 (1H; dd; $J=8.5, 15.0$ Hz; H_6);

7.45 (1H; dt; $J=2.5, 6.0$ Hz; H_3); 7.26 (1H; ddd; $J=2.0, 8.5$ and 15.0 Hz; H_5) ppm. ^{13}C NMR (125.0 MHz, $\text{DMSO-}d_6$) δ : 163.9; 162.5; 163.7 (dd; $J=11.1, 248.6$ Hz); 159.8 (dd; $J=11.0, 159.8$ Hz); 150.4; 139.2; 122.7; 121.2; 118.6 (d; $J=14.5$ Hz); 112.0 (d; $J=21.0$ Hz); 104.8 (t; $J=26$ Hz) ppm. IR (cm^{-1} ; KBr): 3191 (NH); 1610 (CO); 1605 (CO).

Crystals for X-ray diffraction study were obtained by slow crystallization from heptane.

2.1.3. Preparations of 2,4-dichloro-*N'*-isonicotinoylbenzohydrazide hydrochloride [4H^+ , Cl^-]

This was prepared from 2 and isoniazid by a similar procedure as used for 3, except that triethylamine was not used.

Yield: 78%; m.p.: 221–222 $^\circ\text{C}$. ^1H NMR (500.00 MHz, $\text{DMSO-}d_6$) δ : 11.42 (1H; s; NH); 10.84 (1H; s; NH); 9.03 (2H; d; $J=6.0$ Hz; $\text{H}_{2/}$ and $\text{H}_{6/}$); 8.24 (2H; d; $J=6.0$ Hz; $\text{H}_{3/}$ and $\text{H}_{5/}$); 7.79 (1H; s; H_3); 7.61 (1H; d; $J=11.0$ Hz; H_5 or H_6); 7.60 (1H; d; $J=10.0$ Hz; H_5 or H) ppm. ^{13}C NMR (125.0 MHz, $\text{DMSO-}d_6$) δ : 164.5; 162.5; 145.9; 143.6; 135.4; 133.0; 131.7; 130.6; 129.5; 127.4; 123.6 ppm. IR (cm^{-1} ; KBr): 3137 (NH); 1703 (CO); 1668 (CO).

Suitable crystals for the X-ray study were grown from methanol solution and were shown to be the dihydrate [4H^+ , $\text{Cl}^- \cdot 2\text{H}_2\text{O}$].

2.2. X-ray crystallographic study of 3 and [4H^+ , $\text{Cl}^- \cdot 2(\text{H}_2\text{O})$]

The measurements were made at 150 K for 3 and at room temperature for [4H^+ , $\text{Cl}^- \cdot 2(\text{H}_2\text{O})$], on an Enraf-Nonius KAPPA CCD diffractometer (95 mm CCD camera on κ -goniostat) with graphite monochromated $\text{Mo K}\alpha$ ($\lambda=0.71703$ Å) radiation. Data collection (ϕ scans and ω scans with κ offsets) was made using the COLLECT Program [5]; final unit cell parameters based on all reflections, integration and scaling of the reflections intensities were performed with the HKL DENZO SCALEPACK system of programs [6]. The structures were solved using direct methods and refined by full-matrix least squares procedure on F^2 with SHELXS-97 [7].

The asymmetric unit of **3** consists of a single molecule, exhibiting disorder of the *ortho*-fluoro group in the disubstituted phenyl ring. The disorder corresponds to equal occupation of the two possible *ortho* positions, which enable designations to be used of *syn* and *anti* carbonyl oxygen(O1)–*ortho*-fluorine orientations, see Fig. 1. Atom arrangements and the crystallographic numbering scheme for the *syn* arrangement are shown in Fig. 2.

The asymmetric unit of $[4H^+, Cl^-, 2(H_2O)]$ is comprised of two independent cations, two chloride ions and four water molecules. The major difference between the two cations is the orientation of the *o*-Cl group of the disubstituted phenyl ring relative to the nearest carbonyl oxygen. Atom arrangements and the crystallographic numbering scheme are shown in Fig. 3. Again *syn* and *anti* designations [as indicated by C122–O21, and C112–O11, respectively] can be used here (see Fig. 1).

The program WINGX [8] was used to analyze and prepare the data for publication. Crystal data collection procedures and refinement results are presented in Table 1. The molecular representations were prepared using ORTEP [9].

2.3. Computational methods

2.3.1. Conformational analysis

To allow direct theoretical comparison of the different conformations of the cation $[4H^+]$ and the molecule **3**, the later was protonated at the pyridine nitrogen in silico, to give $[3H^+]$ prior to computational analysis. The *anti* conformations of molecule **3** and cation $[4H^+]$, determined in the X-ray crystallographic study, were used as starting geometries for the conformational analysis: that in $[4H^+, Cl^-, 2(H_2O)]$ was denoted as $[4H^+]$ -a and that in **3** as **3-c**.

The ‘search’ module of Sybyl v6.8 modelling package (Tripos, Inc., Illinois, MA) was used to perform a systematic analysis, using a 30° step, in torsion angles 1, 2 and 3 (θ_1 , θ_2 and θ_3 , respectively) as identified in Fig. 1. Molecular mechanics (MM) energies for each of the 1728 conformers for $[3H^+]$ and $[4H^+]$ were calculated in order to evaluate minima in the potential energy surface (PES). Accordingly, the conformers described in Table 5 along with Fig. 5 are designated by numbers reflecting the sequential numeration from 1 through 1728 received during the conformational analysis. MM energies were obtained using the Tripos force field parameters and partial atomic charges accommodated from the electrostatic potential, which was calculated for the X-ray derived geometry with the AM1 Hamiltonian. Also for the purpose of MM calculations, the central hydrazide nitrogen atoms were

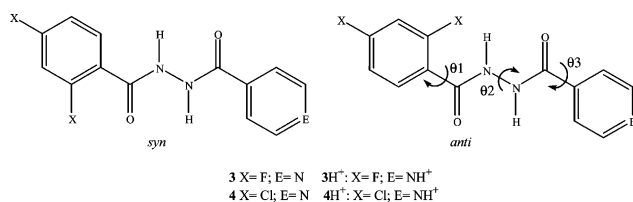


Fig. 1. The *syn* and *anti* forms of **3**, **4**, $[3H^+]$ and $[4H^+]$.

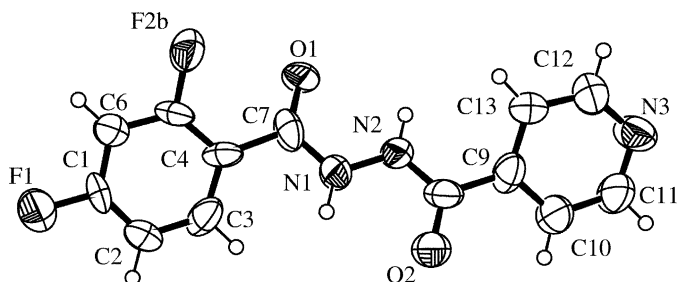


Fig. 2. Atom arrangements and atom numbering scheme for one of the disordered forms [*syn*-conformer] of **3**.

assigned as N_{am} (amide nitrogen) types and the pyridinium ring nitrogen as N_{pl} (trigonal planar nitrogen).

2.3.2. Quantum chemical calculations

All quantum chemical calculations were performed within Gaussian 03, Revision B.01 [10], running on the computational facilities in the Laboratório de Físico-química Orgânica e Modelagem Molecular (Dr Ricardo Bicca De Alencastro, DQO, IQ, Universidade Federal do Rio de Janeiro). Conformers corresponding to symmetry-unique local minima in $[3H^+]$ and $[4H^+]$ PES were subjected to preliminary full optimization with AM1 semi-empirical method and subsequently optimized with Restricted Hartree–Fock theory level and 6-31G* basis set (RHF/6-31G*). Geometries corresponding to RHF/6-31G* local minima were further optimized using density functional theory (DFT) with Becke’s three-parameter functional and the correlation functional of Lee–Yang–Parr (B3LYP) using the standard 6-31G* basis set (DFT-B3LYP/6-31G*). The resulting geometries also had their electronic energies calculated with a larger basis set (DFT-B3LYP/6-311++G**//DFT-B3LYP/6-31G*) for validation of results. Frequency calculations were accomplished for each conformer representing a local minimum in the PES in order to correct for zero-point energy (ZPE) deviation. A single-point supermolecule calculation was attempted based on the

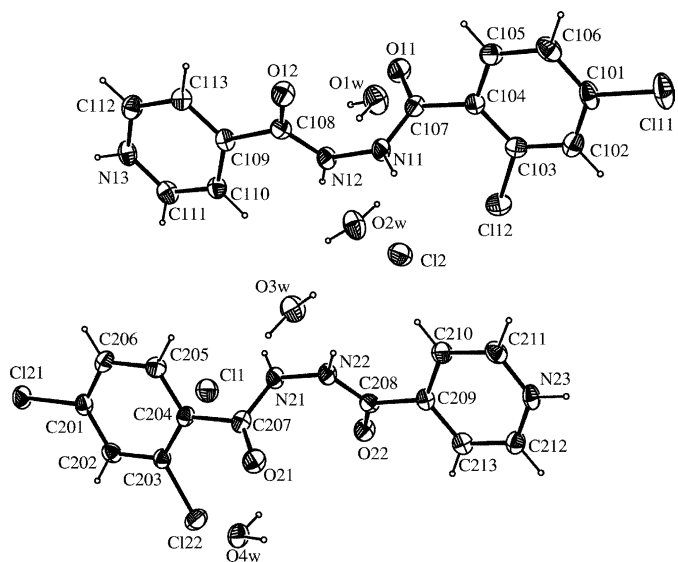


Fig. 3. Atom arrangements and atom numbering scheme for $[4H^+, Cl^-, 2(H_2O)]$.

Table 1
Crystal data and structure refinement for **3** and [4H⁺, Cl⁻·2(H₂O)]

Data	3	[4H ⁺ , Cl ⁻ ·2(H ₂ O)]
Empirical formula	C ₁₃ H ₇ F ₂ N ₃ O ₂	C ₁₃ H ₁₈ Cl ₃ N ₃ O ₆
Formula weight	275.22	382.62
Temperature	150(2) K	293(2) K
Wavelength	0.71073 Å	0.71073 Å
Crystal system	Monoclinic	Monoclinic
Space group	<i>P</i> 2 ₁	<i>P</i> 2 ₁ / <i>n</i>
Unit cell dimensions	<i>a</i> = 4.709(3) Å <i>b</i> = 24.398(16) Å <i>c</i> = 5.281(4) Å $\alpha = \gamma = 90^\circ$ $\beta = 92.54(5)^\circ$	<i>a</i> = 7.2069(3) Å <i>b</i> = 48.5142(18) Å <i>c</i> = 9.4688(3) Å $\alpha = \gamma = 90^\circ$ $\beta = 106.658(1)^\circ$
Volume	606.1(7) Å ³	3171.7(2) Å ³
Z	2	8
Absorption coefficient	0.126 mm ⁻¹	0.601 mm ⁻¹
<i>F</i> (000)	280	1568
Crystal size	0.24 × 0.12 × 0.04 mm ³	0.34 × 0.20 × 0.12 mm ³
Theta range for data collection	3.86–20.00°	3.07–25.00°
Index ranges	–4 < <i>h</i> < 4 –23 < <i>k</i> < 23 –5 < <i>l</i> < 4	–8 < <i>h</i> < 8 –54 < <i>k</i> < 57 –10 < <i>l</i> < 11
Reflections collected	919	14,610
Independent reflections	919 [R(int) = 0.0000]	5525 [R(int) = 0.0466]
Completeness	94.0% (to $\theta = 20.00^\circ$)	99.0% (to $\theta = 25.00^\circ$)
Max. and min. transmission	0.9950 and 0.9705	0.9314 and 0.8219
Refinement method	Full-matrix least-squares on <i>F</i> ²	Full-matrix least-squares on <i>F</i> ²
Data/restraints/parameters	919/1/185	5525/0/415
Goodness-of-fit on <i>F</i> ²	1.078	1.044
Final <i>R</i> indices [<i>I</i> > 2σ(<i>I</i>)]	<i>R</i> 1 = 0.0728, <i>wR</i> 2 = 0.1932	<i>R</i> 1 = 0.0380, <i>wR</i> 2 = 0.0904
<i>R</i> indices (all data)	<i>R</i> 1 = 0.0902, <i>wR</i> 2 = 0.2101	<i>R</i> 1 = 0.0981, <i>wR</i> 2 = 0.0904
Largest diff. peak and hole	0.215 and –0.196 e Å ⁻³	0.443 and –0.287 e Å ⁻³

asymmetric unit of [4H⁺, Cl⁻·(H₂O)] using DFT-B3LYP/6-31+G* either in vacuo or using the IPCM solvation model. The supermolecule was built from eight fragments: two cations, two chloride ions and four water molecules. In vacuo, supermolecule calculations were accompanied by counterpoise correction.

3. Results and discussion

3.1. X-ray structure determinations

As stated in Section 2, the *ortho*-fluorine atom in **3** is disordered over two sites, which leads to *syn* and *anti* designations: the former is shown as an ORTEP [9] representation in Fig. 2. As also indicated in Section 2, the two independent cations in the asymmetric unit of [4H⁺, Cl⁻·2(H₂O)] also exhibit different carbonyl–O *o*-F orientations (see Fig. 3). Bond distances and angles are as expected in both **3** and the cations of [4H⁺, Cl⁻·2(H₂O)]. Comparison of the bond lengths and angles determined by X-ray crystallography for [4H⁺] can be made with calculated values, in Table 2. Bond angles and lengths for **3** are not included here, but have been deposited, as well as anisotropic thermal parameters, in the CCDC, registry number 280895. Related data for [4H⁺, Cl⁻·2(H₂O)] have also been deposited under number 280896. The water molecules and the chloride ions in [4H⁺, Cl⁻·2(H₂O)] participate in an extensive hydrogen

bonding network and the geometric parameters associated with the H-bonds are listed in Table 3.

3.2. Comparison between crystallographic and theoretically optimized structures

Structural optimizations of [3H⁺] and [4H⁺] were initially carried out. The ab initio calculations were performed using the ‘standard’ double-split basis set, 6-31G*, within two levels of theory: the usual Hartree–Fock treatment (RHF) and DFT. In Table 4 are listed the main torsional angles θ_1 , θ_2 and θ_3 , and the electronic energies calculated for the different conformers of [4H⁺] either observed experimentally (‘crystal’, single point calculations) or obtained after full geometric optimizations (optimized). The data show that none of the theoretical methods led to an equilibrium structure strictly identical to that obtained by crystallography. This is clearly perceived from the superposition of the [4H⁺] experimental conformers and their geometry-optimized counterparts in Fig. 4. Such discrepancy suggests that the crystallographic conformers of [4H⁺] are stabilized by inter-species interactions involving the cations, chloride anions and water molecules. A detailed comparison of experimental and optimized geometries for the ‘*anti*’ and ‘*syn*’ cations in [4H⁺, Cl⁻·2(H₂O)] is presented in Table 2. The rmsd of bond lengths between theory and experiment within the ‘*anti*’ conformer geometry, as predicted by RHF and DFT-B3LYP methods, are very similar (0.015 and 0.014 Å,

Table 2
Comparison of calculated structural parameters and experimental (X-ray) for *anti*- and *syn*-[4H⁺]

(a) Bond lengths (Å)						
Bond	Calculated				X-ray values	
	<i>Anti</i>		<i>Syn</i>		<i>Anti</i>	<i>Syn</i>
	RHF/6-31G*	B3LYP/6-31G*	RHF/6-31G*	B3LYP/6-31G*		
CIX1–CX01	1.730	1.741	1.731	1.744	1.736(2)	1.741(3)
CIX2–CX03	1.745	1.764	1.734	1.747	1.739(2)	1.733(2)
OX1–CX07	1.197	1.235	1.191	1.216	1.229(3)	1.216(3)
OX2–CX08	1.185	1.229	1.186	1.215	1.225(3)	1.225(3)
NX1–NX2	1.367	1.373	1.374	1.391	1.384(3)	1.379(3)
NX1–CX07	1.368	1.375	1.387	1.416	1.339(3)	1.357(3)
NX2–CX08	1.365	1.349	1.364	1.378	1.342(3)	1.346(3)
NX3–CX11	1.334	1.353	1.334	1.351	1.341(3)	1.334(3)
NX3–CX12	1.339	1.355	1.339	1.355	1.337(3)	1.336(3)
CX01–CX02	1.382	1.394	1.384	1.395	1.386(4)	1.380(3)
CX01–CX06	1.383	1.396	1.382	1.395	1.382(4)	1.380(3)
CX02–CX03	1.383	1.393	1.382	1.394	1.381(3)	1.384(3)
CX03–CX04	1.393	1.410	1.393	1.409	1.396(3)	1.391(3)
CX04–CX05	1.393	1.409	1.391	1.406	1.392(3)	1.391(3)
CX04–CX07	1.499	1.492	1.496	1.490	1.506(3)	1.503(3)
CX05–CX06	1.379	1.386	1.382	1.390	1.378(3)	1.387(3)
CX08–CX09	1.517	1.505	1.516	1.515	1.506(3)	1.511(3)
CX09–CX10	1.392	1.406	1.392	1.403	1.397(3)	1.396(3)
CX09–CX13	1.393	1.406	1.393	1.404	1.388(3)	1.381(3)
CX11–CX10	1.373	1.382	1.373	1.384	1.372(3)	1.372(3)
CX13–CX12	1.369	1.379	1.369	1.380	1.377(3)	1.373(3)

(b) Bond angles (°)						
Angle ^a	Calculated				X-ray values	
	<i>Anti</i>		<i>Syn</i>		<i>Anti</i>	<i>Syn</i>
	RHF/6-31G*	B3LYP/6-31G*	RHF/6-31G*	B3LYP/6-31G*		
CIX1–CX01–CX02	119.2	119.2	119.2	119.1	118.5(2)	119.25(19)
CIX1–CX01–CX06	119.9	120.0	118.7	119.7	119.9(2)	118.67(19)
CX12–CX03–CX02	116.1	115.0	117.3	117.4	118.46(19)	117.24(19)
CX12–CX03–CX04	122.8	123.5	121.1	121.9	119.91(17)	121.17(19)
OX1–CX07–NX1	120.0	117.4	124.0	120.4	124.0(2)	124.0(2)
OX1–CX07–CX04	122.0	122.3	123.3	125.4	121.9(2)	123.3(2)
OX2–CX08–NX2	125.8	123.3	124.2	125.2	124.0(2)	124.2(2)
OX2–CX08–CX09	119.1	120.7	120.8	119.2	120.7(2)	120.8(2)
NX2–NX1–CX07	118.2	115.2	119.6	116.4	120.99(19)	119.62(19)
NX1–NX2–CX08	117.7	119.6	119.0	117.6	119.14(19)	119.03(19)
NX1–CX07–CX04	118.0	120.4	112.7	114.1	114.0(2)	112.7(2)
NX2–CX08–CX09	115.0	116.0	115.0	115.6	115.3(2)	115.1(2)
CX12–NX3–CX11	123.1	122.8	122.7	123.1	122.8(2)	122.7(2)
NX3–CX11–CX10	119.7	119.6	120.1	119.7	120.0(2)	120.0(2)
NX3–CX12–CX13	119.7	119.4	119.5	119.7	119.4(2)	119.4(2)
CX02–CX01–CX06	121.0	120.8	122.1	121.1	121.6(2)	122.1(2)
CX01–CX02–CX03	119.4	119.5	118.4	119.5	118.3(2)	118.4(2)
CX01–CX06–CX05	118.8	118.8	118.4	118.8	119.2(2)	118.4(2)
CX02–CX03–CX04	121.1	121.5	121.6	120.6	121.6(2)	121.6(2)
CX03–CX04–CX05	117.9	116.9	118.2	118.5	118.3(2)	118.2(2)
CX03–CX04–CX07	127.4	129.2	122.9	122.4	122.6(2)	122.9(2)
CX05–CX04–CX07	114.7	113.8	118.8	119.0	119.0(2)	118.9(2)
CX04–CX05–CX06	121.8	122.5	121.4	121.5	121.0(2)	121.4(2)
CX08–CX09–CX10	123.2	125.5	123.0	123.3	123.0(2)	123.0(2)
CX08–CX09–CX13	116.9	115.6	117.7	116.7	117.6(2)	117.7(2)
CX13–CX09–CX10	119.9	118.8	119.3	119.9	119.4(2)	119.3(2)
CX09–CX10–CX11	118.8	119.6	118.8	118.7	118.9(2)	118.8(2)
CX09–CX13–CX12	118.9	119.8	119.6	118.8	119.5(2)	119.6(2)

^a X=1 for *anti*-[4H⁺] and 2 for *syn*-[4H⁺].

Table 3
Hydrogen bonding parameters for $[4H^+, Cl^- \cdot 2(H_2O)]$

D–H...A	D–H (Å)	D...A (Å)	H...A (Å)	D–H...A (°)
N11–H11–Cl2	0.860	3.119	2.133	160
N12–H12...O2w	0.860	2.741	1.963	150
N22–H22...O3w	0.860	2.791	2.050	144
O1w–H11w...O12	0.855	2.992	2.156	166
O3w–H31w...Cl2	0.759	3.237	2.494	167
O3w–H32w...Cl1	0.949	3.278	2.340	170
O4w–H41w...O21	0.941	2.861	2.020	148
N13–H13...O1w ⁱ	0.860	3.017	2.408	128
N13–H13...Cl2 ⁱ	0.860	3.174	2.483	138
N23–H23...O4w ⁱⁱ	0.860	2.797	2.098	138
O2w–H22w...Cl1 ^{vi}	0.881	3.196	2.317	175
O1w–H12w...O11 ^x	0.912	2.908	2.065	153
O2w–H22w...Cl1 ^{vi}	0.881	3.196	2.317	175
O2w–H21w...Cl2 ^{vi}	0.948	3.257	2.310	178
O4w–H42w...O22 ^x	0.831	2.996	2.177	16,981

Symmetry operations: (i) $x+1, +y, +z+1$; (ii) $x, +y, +z-1$; (vi) $x+1, +y, +z$; (x) $x-1, +y, +z$.

respectively). However, a comparison of the rmsd of the bond angles clearly indicates the RHF method (rmsd 2.0 \AA^2) to be better than the DFT-B3LYP (rmsd 2.9 \AA^2) approach in predicting the compound planar geometries. Similar results were obtained for the ‘syn’ conformers.

Considering again the data in Table 4, one can clearly note that after optimization, energy could be reduced by as much as 0.2 hartree ($\sim 125 \text{ kcal/mol}$). This large improvement in stabilization was completely unexpected, since crystallographic structures usually correspond to local minima in the PES. The origin of this discrepancy could reside in the intermolecular interactions between symmetry-related $[4H^+]$, in the crystal, obviously not captured by calculations made with the isolated conformers in vacuo. As will be discussed in the following sections, this issue was assessed using different methodologies, such as conformational analysis for both $[3H^+]$ and $[4H^+]$ and supermolecule calculations on $[4H^+]$.

Table 4
Electronic energies for the experimental and theoretically optimized conformers of $[4H^+]$

Conformer	θ_1 (°)	θ_2 (°)	θ_3 (°)	E_{el}^a (hartrees)
<i>Anti</i> -RHF				
Crystal	–66.5	85.7	159.9	–1729.70098
Optimized	–37.5	70.4	147.5	–1729.92628
<i>Anti</i> -B3LYP				
Crystal	–66.5	85.7	159.9	–1736.00397
Optimized	0.4	172.3	168.9	–1736.25814
<i>Syn</i> -RHF				
Crystal	–131.6	–82.6	–153.9	–1729.70110
Optimized	–135.2	–66.3	–146.1	–1729.92428
<i>Syn</i> -B3LYP				
Crystal	–131.6	–82.6	–153.9	–1736.00432
Optimized	–145.2	–71.2	–155.3	–1736.24923

^a Energies calculated using the standard 6-31G* basis-set with the methods (RHF or DFT-B3LYP) indicated in the table. E_{el} values under ‘crystal’ rows were obtained from single-point calculations with X-ray geometries.

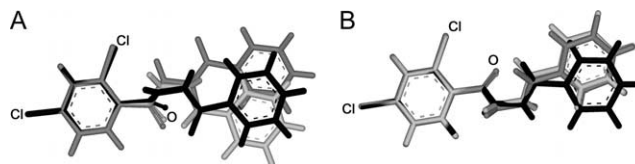


Fig. 4. Comparison between experimental and optimized $[4H^+]$ ‘anti’ (A) and ‘syn’ (B) conformations. Experimental structures are colored in black while structures optimized with either RHF/6-31G* or DFT-B3LYP/6-31G* are colored in light gray or dark gray, respectively. Some of the atoms are labeled to allow for correct orientation.

3.3. Potential energy surfaces (PES)

A systematic conformational analysis of $[3H^+]$ and $[4H^+]$ was accomplished over each of the torsion angles identified in Fig. 1. Variations in amide torsional angles were not considered due to the fact that *cis*-amide geometries were not observed for either **3** or $[4H^+]$ in the X-ray diffraction study. The interdependence of each dihedral angle analyzed was studied from pair-wise contour plots and PES derived for each of the three possible combinations of torsion angles. Comparison of the pattern for each torsion angle in all the generated contour plots indicated a fair degree of independence for θ_1 , θ_2 and θ_3 . As expected, the PESs for each pair-wise combination of torsional angles were very similar for $[3H^+]$ and $[4H^+]$. In general, the θ_1 torsion presented a symmetric potential energy profile with an energy barrier around $\theta_1=0^\circ$ and no marked minimum while assuming most stable values at $\pm 20\text{--}40^\circ$, $\pm 100\text{--}120^\circ$, $\pm 140\text{--}180^\circ$. A more interesting profile is observed for $[3H^+]$ where a clear barrier also exists for $\theta_1=180^\circ$ and another minor barrier at ca. $\theta_1=\pm 90^\circ$. The common barrier around $\theta_1=0^\circ$ can be ascribed to the steric clashes between H–N1 and H–C6 when the planes for the phenyl ring and neighboring amide bond are aligned. On the other hand, the energy profile for the two derivatives indicates differences at $\theta_1=180^\circ$. In $[3H^+]$, θ_1 torsion angle near to 180° places the H–N1 of the adjacent amide linkage in perfect position to make a strong hydrogen bonding interaction with F2. This stabilizing interaction is not so effective in $[4H^+]$, due to the greater size and lower electronegativity of the chlorine atom. Regarding θ_2 , for each of $[3H^+]$ and $[4H^+]$, a deep minimum in the energetic profile is observed at 0° . In this conformation, the molecule’s carbonyl moieties point in the same direction. With respect to θ_3 , a profile similar, but even more featureless, than that for θ_1 is obtained for both analogs.

3.4. Characterization of minimum energy conformers

From the analysis of the PESs for each of $[3H^+]$ and $[4H^+]$, we selected seven conformers at $\theta_2=0^\circ$ and varying θ_1 and θ_3 to be subjected to geometry optimizations with RHF/6-31G*. Results are summarized in Table 5. From the calculations for the conformers of $[3H^+]$, only three unique equilibrium geometries were found: $[3H^+_0080]$, $[3H^+_0217]$ and $[3H^+_0794]$. Noteworthy, none of the equilibrium geometries found for $[3H^+]$ were representative of either crystallographic

Table 5
Relative stabilities of minimum energy conformers for [3H⁺] and [4H⁺]

Conformer	θ_1 (°)	θ_2 (°)	θ_3 (°)	E (hartree)	$E_{\text{ZPE}}^{\text{a}}$ (hartree)	$E_{\text{rel}}^{\text{b}}$ (kcal/mol)
[3H⁺]						
RHF						
0000 ^c	−3.8	−71.3	−56.1	−1009.84209	0.23926	0.0
0217	6.0	69.2	−34.6	−1009.84129	0.23924	0.5
0080	147.8	67.3	57.4	−1009.83493	0.23918	4.4
0222	−141.9	−93.6	−33.3	−1009.83320	0.23893	5.4
DFT-B3LYP						
0000 ^c	−5.5	−71.1	−57.0	−1015.53918	0.22172	0.0 (0.0)
0217	8.4	75.5	−27.2	−1015.53785	0.22156	0.7 (0.4)
0222	−154.2	−156.8	14.2	−1015.53396	0.22095	2.8 (2.4)
0080	152.1	67.3	58.7	−1015.53122	0.22167	5.0 (4.5)
[4H⁺]						
RHF						
1082	−37.5	70.3	147.5	−1729.92627	0.23568	0.0
0227	40.4	68.0	−34.6	−1729.92638	0.23599	0.1
1230	−117.3	69.0	146.7	−1729.92466	0.23556	0.9
0798	−135.2	−66.3	−146.1	−1729.92428	0.23587	1.4
DFT-B3LYP						
0227	21.6	75.5	−27.0	−1736.25280	0.21840	0.0 (0.0)
1082	21.6	75.4	−27.1	−1736.25279	–	0.0 (–)
1230	−129.0	72.1	154.3	−1736.24890	0.21812	2.3 (2.0)
0798	−145.1	−71.3	−155.1	−1736.24923	0.21842	2.3 (2.2)

^a Computed by frequency calculations using the standard basis-set 6-31G* and the methods (RHF or DFT-B3LYP) indicated in the table.

^b Energy relative to the most stable conformer; figures given in parenthesis correspond to the results of DFT-B3LYP/6-311++G**//DFT-B3LYP/6-31G* calculations.

^c Conformer 0000 represents the RHF/6-31G* optimized geometry of [3H⁺]-c.

geometry found by X-ray diffraction data. Moreover, in none of the three equilibrium geometries found for [3H⁺] were the amide linkages *trans* as found in the X-ray structure but these are *gauche* where a higher dipole moment would be expected. These experimental geometries are characterized by a mostly planar conformation with the amide linkages nearly co-planar with both phenyl rings and the central carbonyls *trans* to each other. These differences are somewhat expected since X-ray geometries refer to the *anti* and *syn* conformations of the free base, **3**. Accordingly, for [4H⁺], both conformations given by X-ray diffraction analysis could be found among the four minimum energy conformers obtained by the gas-phase calculations ([4H⁺_0227], [4H⁺_0798], [4H⁺_1082] and [4H⁺_1230]). The [4H⁺_1082] conformer presented a similar geometry to the ‘*anti*’ conformer present in the asymmetric unit cell, while conformer [4H⁺_0798] was equivalent to the ‘*syn*’ conformer (Table 5).

Each of the symmetry-unique equilibrium geometries encountered for [3H⁺] and [4H⁺] using the RHF/6-31G* calculation was subjected to further optimization within the DFT-B3LYP theory level while maintaining the same basis-set. This model would take some account of electron correlation effects, which are completely neglected by the RHF method, at a reasonable computational cost. The electronic and relative energies (corrected for ZPE) for the RHF and DFT-B3LYP optimized final geometries are listed in Table 5. In the case of [3H⁺], most of the conformers retained their geometries after optimization within DFT-B3LYP method, including conformer [3H⁺_0000] (the RHF/6-31G* optimized geometry of [3H⁺]-c). The exception is

[3H⁺_0222] that shows significant deviations in θ_2 and θ_3 upon optimization at the DFT-B3LYP theory level. The relative energies reported in Table 5 also reflect this behavior. The conformer [3H⁺_0000] is predicted to be more stable than the conformers 0217 and 0080 by almost the same amounts with RHF and DFT-B3LYP energy models (0.5–0.7 and 4.4–5.0 kcal/mol, respectively). This result is maintained despite the employment of a much larger basis-set, discarding possible basis-set effects. On the other hand, the results for [3H⁺_0222] differ by more than 1.5 kcal/mol when comparing calculations performed at the two theory levels. This discrepancy actually inverts the stability order regarding [3H⁺] conformers 0080 and 0222 when going from RHF to DFT-B3LYP calculations. Fig. 5 shows the structures for the symmetry-unique [3H⁺_0222] conformers optimized at the DFT-B3LYP (B3LYP) and RHF levels of theory. It can be noted that the conformer obtained after optimization with DFT-B3LYP presents a quite planar structure contrasting with the ‘packed’ geometry, which is furnished by the RHF method.

Regarding [4H⁺], results in Table 5 demonstrate an even more pronounced disagreement in geometries obtained by calculations performed with RHF and DFT-B3LYP energy models. The extreme case is that of the [4H⁺_1082] conformer whose deviation in θ_1 dihedral angle amounts to almost 60° upon optimization with the DFT-B3LYP method. Indeed, the [4H⁺_1082] conformer obtained after DFT-B3LYP geometry optimization is equivalent to the geometry of the 0227 conformer obtained at the same theory level. Interestingly, these conformers are also nearly energetically equivalent at the RHF level, although presenting different geometries as

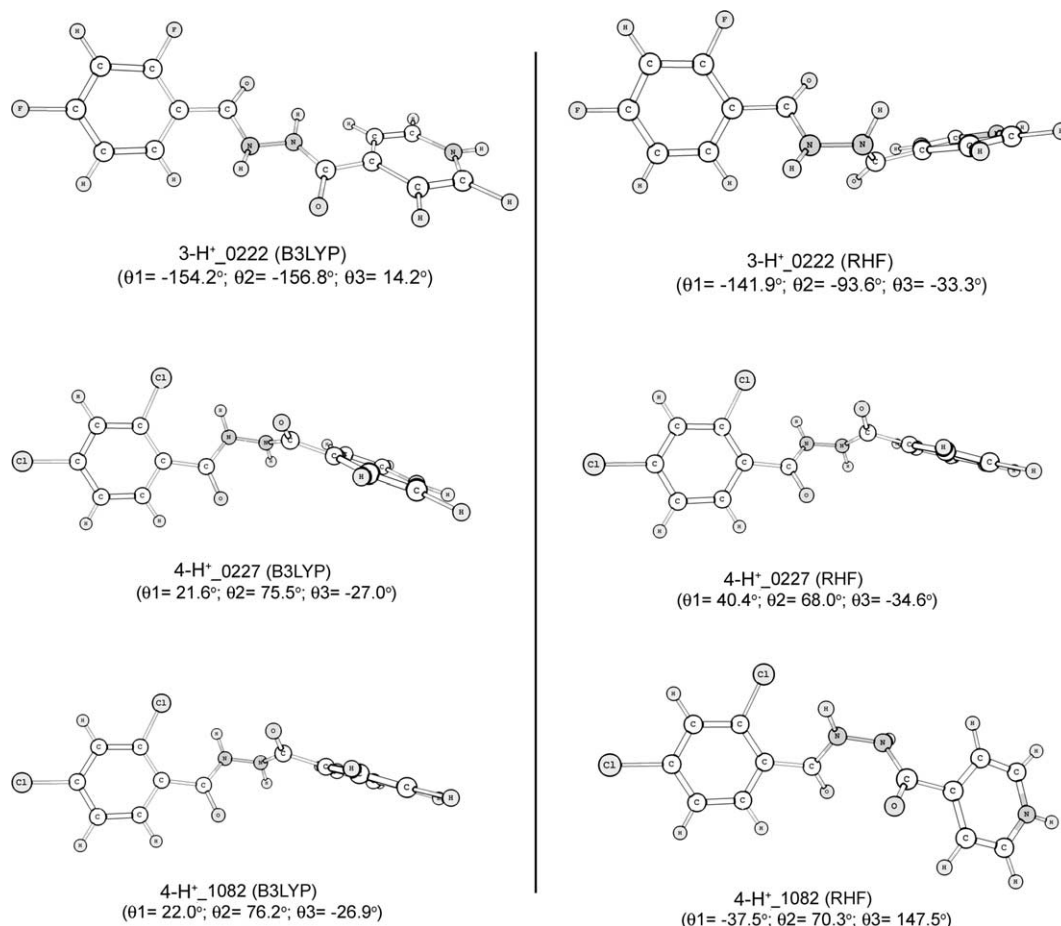


Fig. 5. Comparison of selected minimum energy conformers encountered for $[3\text{H}^+]$ and $[4\text{H}^+]$ at RHF/6-31G* (RHF) and DFT-B3LYP/6-31G* (B3LYP) levels.

depicted by the values of the dihedral angles reported in Table 5 and by the structures in Fig. 5. The results of the calculations with RHF and DFT-B3LYP also disagree over the relative stabilities of the conformers by about 1 kcal/mol, although roughly preserving the relative stability order.

3.5. Supermolecule calculation

Supermolecule calculations are commonly employed to estimate the magnitude of non-covalent interactions in molecular complexes. Accordingly, we have performed this type of calculation with the complex found in the asymmetric unit of crystalline $[4\text{H}^+, \text{Cl}^- \cdot 2(\text{H}_2\text{O})]$ using DFT-B3LYP/6-31+G*. The polarization function was introduced to estimate more properly the interaction energies in the presence of chloride anions while the basis-set superposition error (BSSE) was treated by applying counterpoise correction. The intermolecular interaction energy in $[4 \cdot \text{H}^+, \text{Cl}^- \cdot 2(\text{H}_2\text{O})]$ was estimated to be -175.2 kcal/mol (corrected for BSSE) and the BSSE energy was calculated as 7.0 kcal/mol. The magnitude of this stabilization energy is comparable to the difference between E_{cl} in crystallographic and theoretically optimized $[4\text{H}^+]$ conformers (around 0.2 hartree) and gives support to our previous discussion about the origin of such a discrepancy. It should be clear that this huge stabilization

energy is relative to the calculation performed in vacuo and that a much smaller interaction energy should be expected in a solvated system, mainly due to shielding of the electrostatic interactions. We have actually attempted to make the same supermolecule calculation employing iterated and non-iterated polarization continuum methods (IPCM and PCM, respectively) to estimate, quantum chemically, the solvation enthalpies involved but calculations failed to converge with $[4\text{H}^+, \text{Cl}^- \cdot 2(\text{H}_2\text{O})]$.

4. Concluding remarks

X-ray crystallography and quantum chemical calculations using a standard medium-sized basis-set within two model chemistries were employed to characterize the structures of two halogenated isoniazid derivatives active against the tuberculosis bacilli. In general, DFT-B3LYP model furnished $[4\text{H}^+]$ conformations in better agreement with experiment than the simpler RHF method, possibly due to some account of polarization effects by the former. The results of these calculations also evidenced a high degree of distortion in the geometries of crystallized compounds compared to theoretical gas-phase structures. Supermolecule calculations within the asymmetric unit of crystalline $[4 \cdot \text{H}^+, \text{Cl}^- \cdot 2(\text{H}_2\text{O})]$, using DFT-B3LYP/6-31+G*, suggest that such distorted structures

result from polar and electrostatic interactions within the solvent and other symmetry-related species in the crystal. The characterization of the PES considering three significant dihedral angles showed that the studied isoniazid derivatives present highly flexible structures. In general, an energetic barrier could not be directed for restricted rotation of any of the varied torsion angles at room temperature, even though the fluorinated compound [3H^+] showed an important energy barrier for rotation around θ_1 due to a strong internal hydrogen bond between F4 and H–N6. Differences in electronic energies for the most stable gas-phase conformers were found to amount to a maximum of 2–5 kcal/mol.

This high flexibility may have an impact in the biological activities of these compounds since they are expected to have a significant entropic loss upon binding of these isoniazid derivatives with their, still unrecognized, biological target. In addition, it can be expected that polar interactions within the binding site of the targeted *bacillus* macromolecule can easily impose distortions to the structures of **3** and **4** in order to improve free energy of binding. Isoniazid is a prodrug and must be oxidized by a bacillus peroxidase (KatG) in order to become active. The target of the active isoniazid metabolite is known to be an enoyl–acyl carrier protein reductase from *M. tuberculosis* [11]. Nevertheless, since the site of the chemical modification introduced to render the biologically active isoniazid metabolite match the site of the structural modification used to synthesize compounds **3** and **4**, we cannot rule out the possibility of the biological target of these derivatives be distinct from the parental isoniazid.

Acknowledgements

São Paulo and Rio de Janeiro State Foundations for the Support of Research (FAPESP and FAPERJ) and the National Council for Scientific Research and Development (CNPq) for financial support. FPS Jr thanks to Dr Pierre Mothé Esteves for

fruitful discussions on quantum chemical calculations and Dr Ricardo Bicca for making Gaussian03 available. FPS Jr was a doctoral fellowship recipient from the CNPq. JLW thanks CNPq for financial support.

References

- [1] <http://www.who.int/tdr/>
- [2] <http://www.who.int/tb/en/>
- [3] R.J. Coker, Public Health 117 (2003) 281.
- [4] I. Neves Junior, G.B.P. Miranda, M.C.S. Lourenço, T.R.A. Vasconcelos, K.C. Pais, J.P. Alcântara Jr., M.V.N. Souza, Beilstein Journal of Organic Chemistry, submitted 2005.
- [5] COLLECT: Enraf Nonius, COLLECT, Nonius B.V., Delft, The Netherlands, 1997.
- [6] Z. Ortinowski, W. Minor, in C.W. Carter Jr., R.M. Sweet (Eds.) Methods in Enzymology, HKL DENZO SCALEPACK System of Programs, vol. 276, Academic Press, New York, 1997, p. 307
- [7] G.M. Sheldrick, SHELXS-97, Program for crystal structure solution, University of Göttingen, 1997.
- [8] L.F. Farrugia, Journal of Applied Crystallography 30 (1997) 565.
- [9] L.F. Farrugia, Journal of Applied Crystallography 32 (1999) 837.
- [10] M.J. Frisch, G.W. Trucks, H.B. Schlegel, G.E. Scuseria, M.A. Robb, J.R. Cheeseman, J.A. Montgomery, Jr., T. Vreven, K.N. Kudin, J.C. Burant, J.M. Millam, S.S. Iyengar, J. Tomasi, V. Barone, B. Mennucci, M. Cossi, G. Scalmani, N. Rega, G.A. Petersson, H. Nakatsuji, M. Hada, M. Ehara, K. Toyota, R. Fukuda, J. Hasegawa, M. Ishida, T. Nakajima, Y. Honda, O. Kitao, H. Nakai, M. Klene, X. Li, J.E. Knox, H.P. Hratchian, J.B. Cross, C. Adamo, J. Jaramillo, R. Gomperts, R.E. Stratmann, O. Yazyev, A.J. Austin, R. Cammi, C. Pomelli, J.W. Ochterski, P.Y. Ayala, K. Morokuma, G.A. Voth, P. Salvador, J.J. Dannenberg, V.G. Zakrzewski, S. Dapprich, A.D. Daniels, M.C. Strain, O. Farkas, D.K. Malick, A.D. Rabuck, K. Raghavachari, J.B. Foresman, J.V. Ortiz, Q. Cui, A.G. Baboul, S. Clifford, J. Cioslowski, B.B. Stefanov, G. Liu, A. Liashenko, P. Piskorz, I. Komaromi, R.L. Martin, D.J. Fox, T. Keith, M.A. Al-Laham, C.Y. Peng, A. Nanayakkara, M. Challacombe, P.M.W. Gill, B. Johnson, W. Chen, M.W. Wong, C. Gonzalez, J.A. Pople, GAUSSIAN 03, Revision B.01, Gaussian, Inc., Pittsburgh PA, 2003.
- [11] D.A. Rozwarski, G.A. Grant, D.H.R. Barton, W.R. Jacobs Jr., J.C. Sacchettini, Science 279 (1998) 98–102.